JAERI-M
86-061

AN ANALYSIS OF MULTISLOT
DIRECTIONAL COUPLER

March 1986

Hiroyuki ARAI*, Naohisa GOTO*
and Takumi YAMAMOTO

日 本 原 子 力 研 究 所
Japan Atomic Energy Research Institute

An Analysis of Multislot Directional Coupler

Hiroyuki ARAI*, Naohisa GOTO* and Takumi YAMAMOTO

Department of Thermonuclear Fusion Research

Naka Fusion Research Establishment

Japan Atomic Energy Research Institute

Naka-machi, Naka-gun, Ibaraki-ken

This paper presents an analysis of multislot directional coupler for monitoring the gyrotron output. We solved the boundary value problem of the directional coupler to investigate the detailed effect of finite thickness slot and mutual coupling between slots. Numerical data of coupler design is presented for non-resonant a pair slot, and mode sensitivity in overmoded waveguide is also evaluated.

---

* Department of Physical Electronics, Tokyo Institute of Technology

多スロット方向性結合器

日本原子力研究所那珂研究所核融合研究部
新井　宏之*・後藤　尚久*・山本　　巧

　ジャイロトロン発振出力モニター用として，多スロット方向性結合器の解析について報告する。結合器を電磁界の境界値問題として，数値計算し，スロット部の壁厚さ及びスロット間の相互作用の効果について詳細に検討した。非共振スロット結合器の設計計算を行い，多重モード導波管中でのモード選択性を評価した。

Contents

目　　　　次

1. Introduction

The key factor of ECR (electron cyclotron resonant) plasma heating is monitoring output of Gyrotron to estimate the plasma heating power. It is also necessary to monitor mode composition in the overmoded waveguide, since reflected waves from the plasma cause much higher mode in overmoded waveguide of Gyrotron output. For monitoring the Gyrotron output, multi-hole directional coupler have been used [1] [2], however the rigorous theoretical approach has not been obtained.

The directional coupler may be also composed of slot instead of hole, and the slot coupler is easy to calculate its performance rigorously. This paper presents the analysis of multislot directional coupler to calculate rigorously the effect of wall thickness and the mutual coupling between slots. We derive a set of integral equation for the directional coupler and solve it by using the method of moments in the following section. Sec. 3 presents numerical data for the design of directional coupler consisting of a pair slot. Mode selectivity of the coupler is discussed in Sec. 4. This paper concludes with discussion and future problem.

2. Formulation

Bethe [3] developed originally the theory of microwave coupling by small aperture of zero thickness. Cohn [4] described a major extension of Bethe's work, and enabled the theory to apply large aperture of finite thickness. Levy applied Bethe-Cohn theory to multiaperture couplers [5], and also showed the theory of including the mutual interactions [6]. Meanwhile, MacDonald [7] presented thickness correction factor obtained by the resonator model. However, these analysis of couplers are for the single mode waveguide, and are not verified for the overmoded waveguide.

In this section, we solve the boundary value problem of the multislot directional coupler to investigate the detailed effect of finite thickness slot and the mutual coupling between slots. This is almost based on Seki's formulation [8]. Fig. 1 (a) illustrates the overall configuration of our analysis model. The directional coupler consists of multislot located between a rectangular and a overmoded circular waveguide. For

1. Introduction

The key factor of ECR (electron cyclotron resonant) plasma heating
is monitoring output of Gyrotron to estimate the plasma heating power.
It is also necessary to monitor mode composition in the overmoded wave-
guide, since reflected waves from the plasma cause much higher mode in
overmoded waveguide of Gyrotron output. For monitoring the Gyrotron
output, multi-hole directional coupler have been used [1] [2], however
the rigorous theoretical approach has not been obtained.

The directional coupler may be also composed of slot instead of hole,
and the slot coupler is easy to calculate its performance rigorously.
This paper presents the analysis of multislot directional coupler to
calculate rigorously the effect of wall thickness and the mutual coupling
between slots. We derive a set of integral equation for the directional
coupler and solve it by using the method of moments in the following
section. Sec. 3 presents numerical data for the design of directional
coupler consisting of a pair slot. Mode selectivity of the coupler is
discussed in Sec. 4. This paper concludes with discussion and future
problem.

2. Formulation

Bethe [3] developed originally the theory of microwave coupling by
small aperture of zero thickness. Cohn [4] described a major extension
of Bethe's work, and enabled the theory to apply large aperture of
finite thickness. Levy applied Bethe-Cohn theory to multiaperture
couplers [5], and also showed the theory of including the mutual
interactions [6]. Meanwhile, MacDonald [7] presented thickness
correction factor obtained by the resonator model. However, these
analysis of couplers are for the single mode waveguide, and are not
verified for the overmoded waveguide.

In this section, we solve the boundary value problem of the multislot
directional coupler to investigate the detailed effect of finite thickness
slot and the mutual coupling between slots. This is almost based on
Seki's formulation [8]. Fig. 1 (a) illustrates the overall configuration
of our analysis model. The directional coupler consists of multislot
located between a rectangular and a overmoded circular waveguide. For

the generalization of the analysis, we consider multi-slot coupler, where the number of slot is N. In our analysis, following assumptions are first assumed.

(1) directional coupler and overmoded circular waveguide have perfectly conducting walls.

(2) a slot is rectangular shape, and its width is much smaller than its length.

(3) each slot direction is in the waveguide axis.

(4) radius of circular waveguide is much larger than the guide wavelength.

The assumption (1) indicates that infinite summation of complete orthogonal mode express the fields in this system. By the slot shape condition (2), the electric field in the slot aperture has a component only in the direction of slot width and the aperture magnetic field has a component only in the direction of slot length. The condition (3) also restricts scattered fields in circular and rectangular waveguide to the transverse electric (H) mode. Finally, by the assumption (4), the surface consisting of slot aperture is regarded as a plane for the simplicity of calculation. All these assumptions are reasonable in our analysis of this directional coupler. Solving this problem gives the fields in the rectangular and the circular waveguide to evaluate the coupling factor.

As a preliminary step, we express magnetic fields in both waveguides and inside the slot by dyadic Green's functions G derived by Collin [9] and the equivalent magnetic current $E_j \times \hat{n}$. The E_j and $\hat{n}$ denote the unknown electric field in the j th slot aperture and a unit vector in the $-y$ direction, respectively. The magnetic fields in the circular waveguide have an incident magnetic field h(r) form the $-z$ direction and scattered magnetic fields excited by the equivalent magnetic current of each slot. On the other hand, the magnetic fields in the rectangular waveguide are expressed by scattered magnetic fields only.

$$H^C(r) = h(r) + \sum_{k=1}^{N} \int \int G^C(r/r_o) \cdot [E_k^C \times \hat{n}] ds_C \tag{1}$$

$$H^R(r) = \sum_{k=1}^{N} \int \int G^R(r/r_o) \cdot [-E_k^R \times \hat{n}] ds_R \tag{2}$$

where the C and R denote circular and rectangular waveguide. In above expression, vectors r and r_o are for an observation point and a source point, respectively.

The magnetic fields inside the j th slot has scattered field from both side of slot aperture and is,

$$H_j(r) = \int \int G_j(r/r_o) \cdot [-E_j^C(r_o) \times \hat{n}] ds_C + \int \int G_j(r/r_o) \cdot [E_j^R(r_o) \times \hat{n}] ds_R \qquad (3)$$

where G_j is the dyadic Green's function in the j th slot. Note that Green's functions in (1)-(3) are those for magnetic fields. Electric fields in the system can be also obtained by changing these Green's functions and the incident field to those for electric fields.

Now we derive a set of integral equation for the directional coupler using the above expression. The continuity condition for the tangential magnetic fields gives the integral equation of j th slot aperture on circular waveguide side S_j^C as,

$$h(r) + \sum_{k=1}^{N} \int \int G^C(r/r_o) \cdot [E_k^C(r_o) \times \hat{n}] ds_C$$

$$= - \int \int G_j(r/r_o) \cdot [E_j^C(r_o) \times \hat{n}] ds_C + \int \int G_j(r/r_o) \cdot [E_j^R(r_o) \times \hat{n}] ds_R \qquad (4)$$

and on the rectangular waveguide side S_j^R as,

$$\int \int G_j(r/r_o) \cdot [E_j^R(r_o) \times \hat{n}] ds_R - \int \int G_j(r/r_o) \cdot [E_j^C(r_o) \times \hat{n}] ds_C$$

$$= - \sum_{k=1}^{N} \int \int G^R(r/r_o) \cdot [E_k^R(r_o) \times \hat{n}] ds_R. \qquad (5)$$

We can evaluate unknown electric fields in each slot aperture by solving the above set of integral equation. To solve this set of integral equation for electric fields in slot aperture, each aperture electric field

is expanded in a series of basis function $g_j(\xi)$ and $f_{jq}(\eta)$ (q=1,2,3) as,

$$E_j = \hat{x} g_j(\xi) \sum_{q=1}^{3} v_{jq}^i f_{jq}(\eta), \qquad (i = C, R) \qquad (6)$$

where v's are unknown expansion coefficients of electric field in each slot aperture. The local coordinate system of the j th slot is shown in Fig. 1 (b). Basis functions for $f_j(\eta)$ and $g_j(\xi)$ should express effectively the nature of electric fields in the slot aperture. Considering the duality between a slot on an infinite plane of perfect conductor and a dipole antenna, we chose following functions for $f_{jq}(\xi)$.

$$f_{j1}(\eta) = \sin\{k_o(L_j - |\eta|)\}]/\sin(k_o L_j) \qquad (7)$$

$$f_{j2}(\eta) = [1 - \cos\{k_o(L_j - |\eta|)\}]/\{1 - \cos(k_o L_j)\} \qquad (8)$$

$$f_{j3}(\eta) = \text{sgn}(\eta)\{f_{j1}(\eta) - f_{j2}(\eta)\} \qquad (9)$$

where sgn(η) takes +1 for $\eta > 0$ and -1 otherwise.

By the analogy of a quasistatic solution for the electric fields across an infinite length slit in a perfect conducting plane with zero thickness [10], the electric field distribution for $g(\xi)$ is given as,

$$g_j(\xi) = (w_j^2 - \xi^2)^{-1/2}. \qquad (10)$$

After substituting (6) into (4) and (5), we employed one of the method of moments, especially Galerkin's method, so as to make a set of linear equations. Both sides of resultant equations are first scalar multiplied with $g_i(\xi) f_{ip}(\eta)\hat{n}$, and are integrated over S_i. Then we obtain the following set of linear equations.

$$\sum_{j=1}^{N} \sum_{q=1}^{3} [v_{jq}^C({}^{C}Y_{ij}^{pq} + \delta_{ij} {}^{C}y_i^{pq}) + v_{jq}^R \delta_{ij} {}^{x}y_i^{pq}] = C_{ip} \qquad (11)$$

$$\sum_{j=1}^{N} \sum_{q=1}^{3} [v_{jq}^{R}({}^{R}Y_{ij}^{qp} + \delta_{ij}{}^{R}y_{i}^{pq}) + v_{jq}^{c}\delta_{ij}{}^{x}y_{i}^{pq}] = 0 \ , \tag{12}$$

$$(j = 1, 2, ..., N, \ p = 1, 2, 3)$$

where δ_{ij} is the Kronecker's delta : δ_{ij} = 1 (i=j), =0 (i≠j). The coefficients Y_{ij}, y_{ij} and C_{ip} are referred to as "generalized admittance ratios" and "a moment of excited magnetic fields" respectively, and are defined as follows [11].

$$^{k}Y_{ij}^{pq} = -Z_{o} \underset{S_{k}\ S_{k}}{\int\int\int\int} g_{i}(\xi)f_{ip}(\eta)\hat{z}\cdot G^{k}\cdot\hat{z}g_{j}(\xi_{o})f_{jq}(\eta_{o})ds_{o}ds \tag{13}$$

$$^{k}y_{ij}^{pq} = -Z_{o} \underset{S_{k}\ S_{k}}{\int\int\int\int} g_{i}(\xi)f_{ip}(\eta)\hat{z}\cdot G\cdot\hat{z}g_{j}(\xi_{o})f_{jq}(\eta_{o})ds_{o}ds \tag{14}$$

$$^{x}y_{ij}^{pq} = Z_{o} \underset{S_{C}\ S_{R}}{\int\int\int\int} g_{i}(\xi)f_{ip}(\eta)\hat{z}\cdot G\cdot zg_{j}(\xi_{o})f_{jq}(\eta_{o})ds_{o}ds \tag{15}$$

$$C_{ip} = Z_{o} \underset{S_{C}}{\int\int} g_{i}(\xi)f_{ip}(\eta)h(r)\hat{z}ds \ , \qquad (k = C,R) \tag{16}$$

where Z_{o} is the wave impedance of free space. The detailed evaluation of Y_{ij}, y_{ij} and C_{i} are listed in Appendix A.

Generalized admittance ratios and the moment of excited magnetic fields are calculated by equations (13)-(16) using Green's functions and basis functions (7)-(10). They determine the set of linear equations (6) for unknown expansion coefficients v's. Finally, the coupling power is obtained by calculating Poynting power in the rectangular waveguide (See Appendix B).

3. Design of directional coupler

This section will present numerical results obtained by our analysis for the design of a pair slot directional coupler. The directional coupler composed of a rectangular waveguide (3.556 × 7.112 mm), and its narrow side is attached to the 32GHz overmoded circular waveguide with its radius

$$\sum_{j=1}^{N} \sum_{q=1}^{3} [v_{jq}^{R}({}^{R}Y_{ij}^{qp} + \delta_{ij}\,{}^{R}y_{i}^{pq}) + v_{jq}^{c}\delta_{ij}\,{}^{x}y_{i}^{pq}] = 0 \ , \tag{12}$$

$$(j = 1, 2, \ldots, N, \ p = 1, 2, 3)$$

where δ_{ij} is the Kronecker's delta : $\delta_{ij} = 1$ (i=j), =0 (i≠j). The coefficients Y_{ij}, y_{ij} and C_{ip} are referred to as "generalized admittance ratios" and "a moment of excited magnetic fields" respectively, and are defined as follows [11].

$$^{k}Y_{ij}^{pq} = -Z_{o} \int\int\int\int_{S_{k}\ S_{k}} g_{i}(\xi) f_{ip}(\eta)\hat{z}\cdot G^{k}\cdot\hat{z}g_{j}(\xi_{o}) f_{jq}(\eta_{o})ds_{o}ds \tag{13}$$

$$^{k}y_{ij}^{pq} = -Z_{o} \int\int\int\int_{S_{k}\ S_{k}} g_{i}(\xi) f_{ip}(\eta)\hat{z}\cdot G\cdot\hat{z}g_{j}(\xi_{o}) f_{jq}(\eta_{o})ds_{o}ds \tag{14}$$

$$^{x}y_{ij}^{pq} = Z_{o} \int\int\int\int_{S_{C}\ S_{R}} g_{i}(\xi) f_{ip}(\eta)\hat{z}\cdot G\cdot zg_{j}(\xi_{o}) f_{jq}(\eta_{o})ds_{o}ds \tag{15}$$

$$C_{ip} = Z_{o} \int\int_{S_{C}} g_{i}(\xi) f_{ip}(\eta)h(r)\hat{z}ds \ , \qquad (k = C,R) \tag{16}$$

where Z_{o} is the wave impedance of free space. The detailed evaluation of Y_{ij}, y_{ij} and C_{i} are listed in Appendix A.

Generalized admittance ratios and the moment of excited magnetic fields are calculated by equations (13)-(16) using Green's functions and basis functions (7)-(10). They determine the set of linear equations (6) for unknown expansion coefficients v's. Finally, the coupling power is obtained by calculating Poynting power in the rectangular waveguide (See Appendix B).

3. Design of directional coupler

This section will present numerical results obtained by our analysis for the design of a pair slot directional coupler. The directional coupler composed of a rectangular waveguide (3.556 × 7.112 mm), and its narrow side is attached to the 32GHz overmoded circular waveguide with its radius

34.5mm. The slot thickness is fixed to 0.9mm except the calculation of coupler's performance dependence on the slot thickness. Fig. 2 shows the slot parameters on the narrow side b of rectangular waveguide, such as, slot spacing, length, width, offset and slot thickness. In addition, frequency characteristics of the coupler is also presented. All the numerical results in this section are calculated in case of the TE_{01} mode incident.

3.1 Slot spacing

First, we define the equivalent guide wavelength so as to normalize the slot spacing dimension. This factor can also give a principle design of the directional coupler. In case of loose-coupling with zero thickness slot and no mutual coupling between slots, we can adopt a principle design for the coupler. With reference to Fig. 3(a), the slot spacing D is defined to cancel the backward wave as,

$$D = \frac{(2n-1) \lambda_e}{4}, \qquad (n = 1, 2, 3, \ldots) \tag{11}$$

$$\lambda_e = \frac{2\lambda_{gC}\lambda_{gR}}{\lambda_{gC} + \lambda_{gR}} \tag{12}$$

where λ_{gC} and λ_{gR} represent the guide wavelength in circular and rectangular waveguide, respectively. The guide wavelength in the circular waveguide should be chosen to that of the wanted mode. In (12), we call λ_e as the equivalent guide wavelength for forward coupling.

In like manner, the equivalent guide wavelength λ_e^+ for backward coupling shown in Fig. 3 (b) is given as,

$$D = \frac{(2n-1) \lambda_e^+}{4}, \qquad (n = 1, 2, 3, \ldots) \tag{13}$$

$$\lambda_e^+ = \frac{2\lambda_{gC}\lambda_{gR}}{\lambda_{gC} - \lambda_{gR}} \tag{14}$$

By the principle design, the zero thickness slot and no mutual coupling, eqs. (11) and (13) define the slot spacing D. For the comparison between the principle design and our analysis, slot spacing is normarized by the equivalent guide wavelength of forward coupling in this paper.

Now we present the performance of directional coupler dependence on the slot spacing. In the following example, a pair slot is composed of the same one and is arrayed in the z axis. Fig. 4 shows coupling coefficient as a function of slot spacing normalized by λ_e for a resonant slot. At the point marked by arrow, forward waves are cancelled in the principle design (D = 0.75 λ_e^+). Difference between dashed and dotted curves gives the directivity of the coupler. In Fig. 4, numerical results are different from the principle design, and the directivity is too low for the small D. These results indicate that the mutual coupling between slots dependence on the higher mode in circular waveguide can not be neglected for the resonant slot. Therefore, we should chose the non-resonant slot to get high directivity.

Fig. 5 shows the coupling coefficient as a function of slot spacing for a non-resonant slot. The principle design can explain these results more accurately than that of the resonant slot. The high directivity, more than 20dB, is obtained in both case of forward and backward coupling for the non-resonant slot. Since the large slot spacing, large number of n in eqs. (11) and (13), generally reduces the frequency band width [12], we should design the slot spacing to be the smallest one. The band width of frequency is also discussed later.

From Figs. 4 and 5, we conclude that the non-resonant slot is more efficient than the resonant slot at the point of directivity for the small D. In the non-resonant slot, the principle design is also verified.

3.2 Slot length, width and offset

This section will discuss slot parameters. Fig. 6 shows the coupling dependence on one slot #2 length at the first, where the other slot (#1) length is fixed to be 3.0mm. Since this case is the forward coupling, the backward coupling mainly changes. If the #2 slot is designed to be 3.0mm, for example, the capacity of manufacturing error of #2 slot is ±0.05mm (1.5%) to suppress the directivity change within 0.5dB.

Next parameter, slot width, is shown in Fig. 7. The change of slot width is performed within the range of assumption (2). As is almost same with the slot length, the width changing of 0.5dB coupling is 0.3mm±0.045mm.

In Figs. 6 and 7, only #2 slot parameter is changed. However the performance of the coupler with #1 slot parameters is changed almost same with that in these figures.

Fig. 8 shows the last parameter, slot offset from the rectangular waveguide axis. In Fig. 8 (a), a pair slot is shifted together. The close location of slot to the rectangular waveguide wall increase the coupling by 3dB. On the other hand, the change in coupling is very small near the central axis because of the symmetry. Figs. 8 (b) and (c) show the coupling performance in case of one slot offset from the center. The ±1.0mm offset causes the coupling change of 0.5dB for both cases. The slot offset does not cause much change of coupling compared with the length and width, which also indicate a amplitude weighting by slot offset is not effective for coupling control.

3.3 Slot thickness

One of the purpose of this paper is to estimate the detailed effects of wall thickness. Fig. 9 shows the coupling dependence on the slot thickness for non-resonant a pair slot. The thick slot reduce the coupling, however, increase the directivity. The decrease in backward coupling by finite thickness slot is larger than that of forward, for example, the slot thickness 0.9mm reduces the forward coupling by 10dB and backward coupling by 20dB. This effect is not explained by the single mode approximation, and is the key feature of our integral equation approach.

3.4 Frequency characteristics

We have examined the slot parameters in the preceding section. Now the coupling dependence on frequency is presented for two length of slot spacing. Fig. 10 shows the results. In Fig. 10, we have plotted data discretely, because the change of frequency makes a new higher mode in the overmoded circular waveguide and causes the discrete of curves. Fig. 10 (a), curves for $D = 0.75\lambda_e$, has more than 20dB directivity in the frequency range of 34.4 ∿ 35.5GHz. In Fig. 10 (b), frequency range of the same directivity is 34.7 ∿ 35.1GHz for $D = 1.25\lambda_e$. These results indicate that we should take the small D for the wide band width.

4. Mode selectivity

In the preceding section, the performance of a pair slot directional coupler is shown for TE_{01} mode incident. It is necessary to know the exact gyrotron output mode mixture mainly consisting of TE_{0m} modes. In this section, we will show the TE_{0m} mode selectivity of a pair slot coupler discussed before. We also present the example of the coupler design for the good mode selectivity.

Fig. 11 shows TE_{0m} mode selectivity. Configuration of directional coupler is the same with that of Fig. 10(a). The directivity is on the decrease by the mode order 6, and mode selectivity is very small. This deficient mode selectivity is the cause that the phase velocity in the rectangular waveguide is not coincide with that of the wanted mode in the circular waveguide. If both waveguides have the same phase velocity, the forward coupling has maximum for the wanted mode. To verify this explanation, we show the example of the directional coupler for TE_{05} mode.

Fig. 12 shows the mode selectivity of a directional coupler designed for TE_{05} mode. The dimension of rectangular waveguide is changed to 6.5805×3.2903 mm to satisfy the above condition that the phase velocity of dominant mode in the rectangular waveguide coincide with that of TE_{05} mode in circular waveguide. In Fig. 12, the TE_{05} mode has much higher directivity than other modes, which indicates the validity of the above explanation. However this design according to the phase velocity does not always apply to other wanted mode in circular waveguide. For example, the design for TE_{01} mode requires the width of rectangular waveguide to be 2.829 mm. Unfortunately, this guide width causes higher mode in the rectangular waveguide, and this design fails for TE_{01} mode.

5. Discussion

We have presented the formulation of the multislot directional coupler for monitoring the gyrotron output. Numerical results show that the non-resonant a pair slot has higher directivity than the resonant one for small slot spacing. For the design of non-resonant slot directional coupler, the accuracy of slot length and width are more important than the slot offset. Though the finite thickness slot reduces the coupling, its directivity is increased. Since the single mode approximation can not explain this result, our analysis is useful for the directional coupler

4. Mode selectivity

In the preceding section, the performance of a pair slot directional coupler is shown for TE_{01} mode incident. It is necessary to know the exact gyrotron output mode mixture mainly consisting of TE_{0m} modes. In this section, we will show the TE_{0m} mode selectivity of a pair slot coupler discussed before. We also present the example of the coupler design for the good mode selectivity.

Fig. 11 shows TE_{0m} mode selectivity. Configuration of directional coupler is the same with that of Fig. 10(a). The directivity is on the decrease by the mode order 6, and mode selectivity is very small. This deficient mode selectivity is the cause that the phase velocity in the rectangular waveguide is not coincide with that of the wanted mode in the circular waveguide. If both waveguides have the same phase velocity, the forward coupling has maximum for the wanted mode. To verify this explanation, we show the example of the directional coupler for TE_{05} mode.

Fig. 12 shows the mode selectivity of a directional coupler designed for TE_{05} mode. The dimension of rectangular waveguide is changed to 6.5805×3.2903 mm to satisfy the above condition that the phase velocity of dominant mode in the rectangular waveguide coincide with that of TE_{05} mode in circular waveguide. In Fig. 12, the TE_{05} mode has much higher directivity than other modes, which indicates the validity of the above explanation. However this design according to the phase velocity does not always apply to other wanted mode in circular waveguide. For example, the design for TE_{01} mode requires the width of rectangular waveguide to be 2.829 mm. Unfortunately, this guide width causes higher mode in the rectangular waveguide, and this design fails for TE_{01} mode.
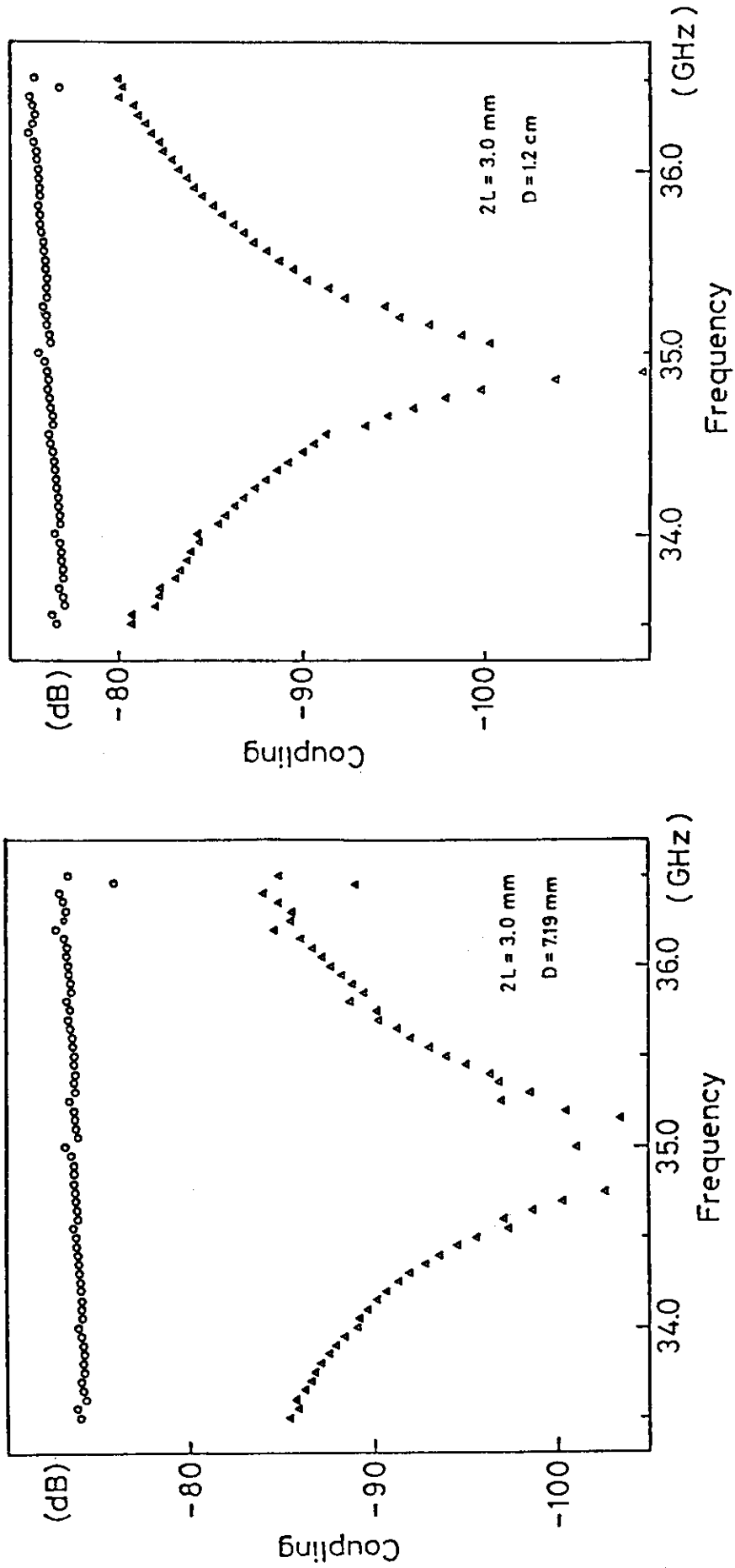
5. Discussion

We have presented the formulation of the multislot directional coupler for monitoring the gyrotron output. Numerical results show that the non-resonant a pair slot has higher directivity than the resonant one for small slot spacing. For the design of non-resonant slot directional coupler, the accuracy of slot length and width are more important than the slot offset. Though the finite thickness slot reduces the coupling, its directivity is increased. Since the single mode approximation can not explain this result, our analysis is useful for the directional coupler

monitoring gyrotron output.

Our analysis includes all mode in the overmoded circular waveguide and is valid for any mode incident. We presented TE_{0m} mode selectivity only, however it is easy to apply this method for asymetrical mode. The mode selectivity was improved by changing the rectangular waveguide dimension, however this is not useful for the practical design. The good mode selectivity is also expected for three or four slot coupler. Our method is useful to simulate the mode selectivity for changing parameters of multislot coupler. The future problem is the design of multislot coupler with good mode selectivity.

Achnowledgements

(a) D=7.19mm

(b) D=12.0mm

Fig. 10 Coupling as a function of frequency

$2L_1=2L_2=3.0mm$, $W_1=W_2=0.1L_1$, $H = 0.5b$, solid line is
forward coupling, dashed line is backward coupling

monitoring gyrotron output.

Our analysis includes all mode in the overmoded circular waveguide and is valid for any mode incident. We presented TE_{0m} mode selectivity only, however it is easy to apply this method for asymetrical mode. The mode selectivity was improved by changing the rectangular waveguide dimension, however this is not useful for the practical design. The good mode selectivity is also expected for three or four slot coupler. Our method is useful to simulate the mode selectivity for changing parameters of multislot coupler. The future problem is the design of multislot coupler with good mode selectivity.

References

[1] G. Janzen, et. al., "Mode selective high power measurements on a
     28GHz gyrotron," 8th. Int. Conf. on Infrared and Millimeter Waves,
     Maiami Beach, Fl., 1983.

[2] G. Janzen and H. Stickel, "Improved directional couplers for
     overmoded waveguide systems," 9th. Int. Conf. on Infrared and
     Millimeter Waves, Takarazuka, 1984.

[3] H.A. Bethe, "Theory of diffraction by small holes," Phys. Rev.
     vol. 66, pp.163-699, Oct. 1944.

[4] S.B. Cohn, "Microwave coupling by large apertures," Proc. IRE,
     vol.4, pp.696-699, June 1952.

[5] R. Levy, "Analysis and synthesis of waveguide multiaperture
     directional couplers," IEEE Trans. MTT, vol. MTT-16, pp995-1006,
     Dec. 1952.

[6] R. Levy, "Improved single and multiaperture waveguide coupling
     theory, including explanation of mutual interactions," IEE Trans.
     MTT, vol. MTT-28, pp.331-338. April 1980.

[7] N. A. McDonald, "Electric and magnetic coupling through small
     apertures in shield walls of any thickness," IEEE trans. MTT,
     vol. MTT-20, pp.689-695. Oct. 1972.

[8] H. Seki, "Moment and variational analysis of slotted waveguide
     antennas and its applications," Doctoral Dissertation, Faculty of
     Engineering, Tokyo Inst. of Technology, December 1981.

[9] R.E. Collin, Fields Theory of Guided Waves, Secs. 5. McGraw Hill
     N.Y. 1960.

[10] W.R. Smyth, Static and Dynamic Electricity, Prob. 4.21, MacGraw
     Hill, N.Y. 1950.

[11] T. Takeda, "A study of directional coupler composed of circular
     and rectangular waveguide," Thesis, Tokyo Inst. of Technology, 1982.

[12] F. Oguchi, Microwave and Milimeterwave Circuit, Maruzen, 1964.
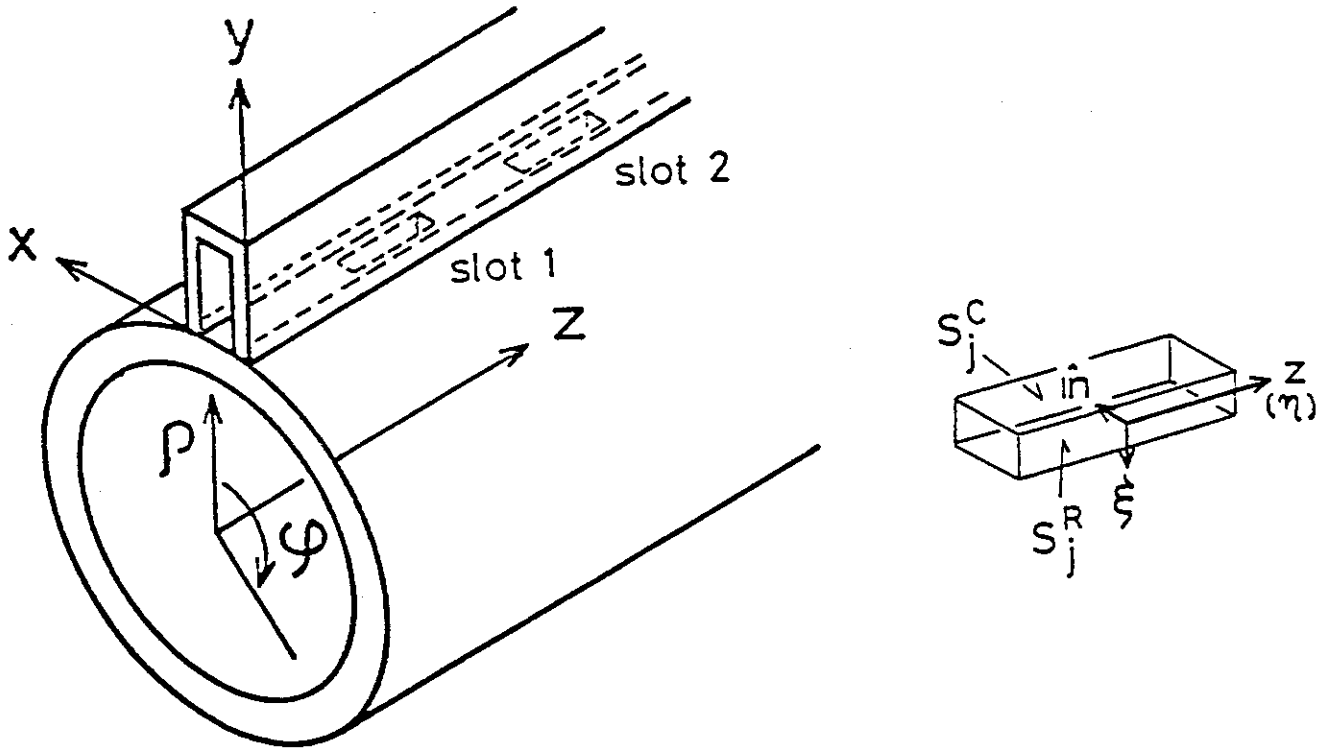
(a) Coordinate system of directional coupler

(b) Coordinate system inside slot

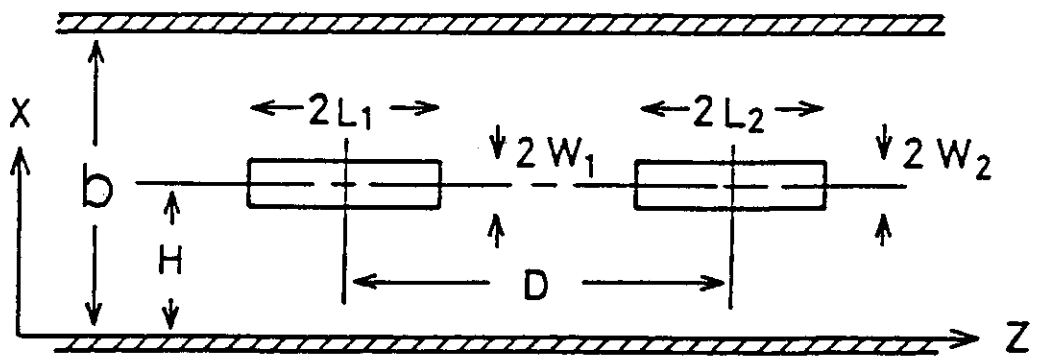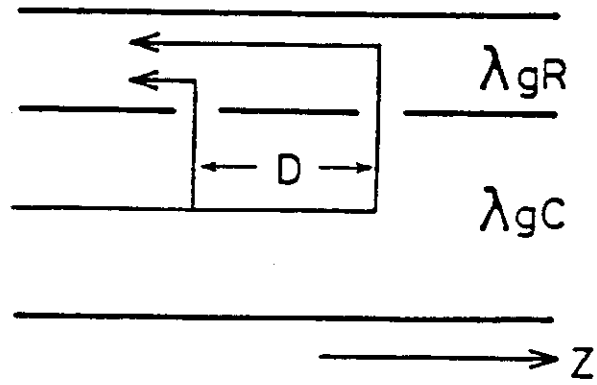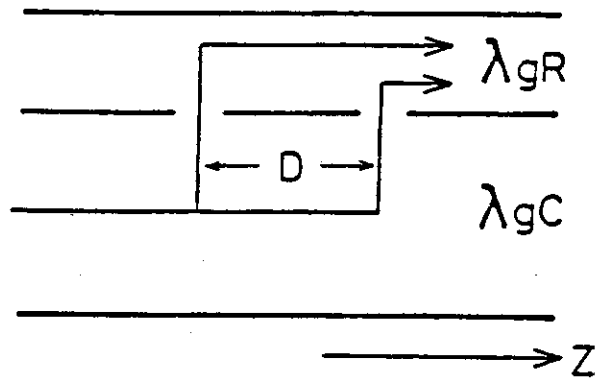Fig. 1 Configularion of slot directional coupler

Fig. 2 Slot parameters

(a) backward wave
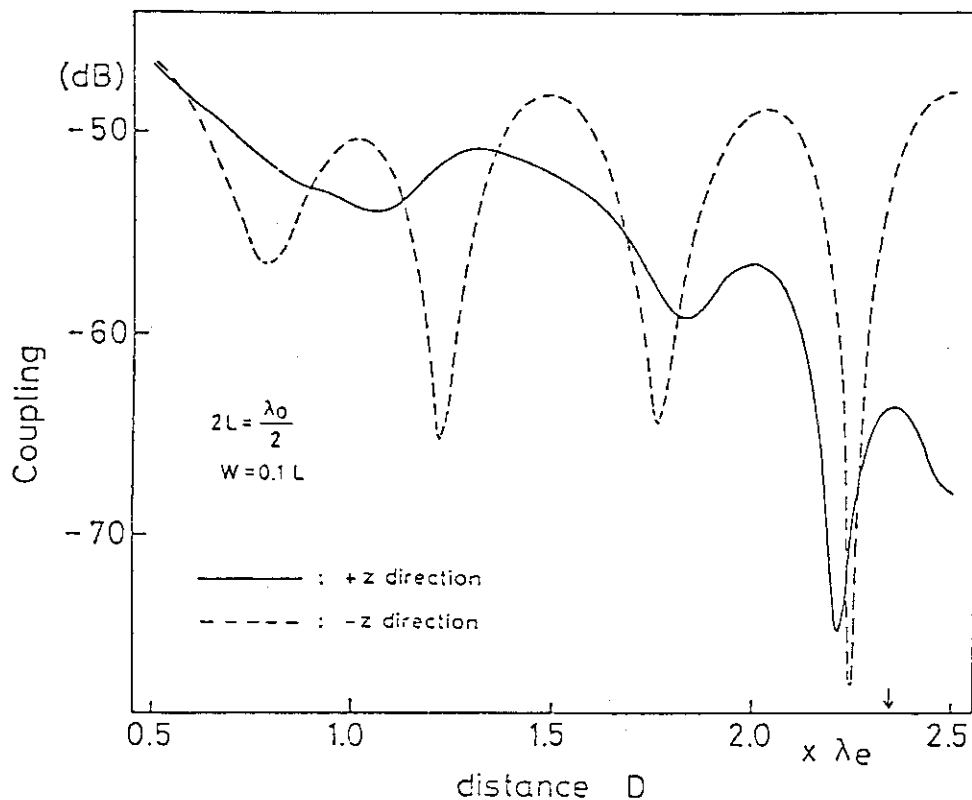

(b) forward wave

Fig. 3   Skecth of cancelled wave

Fig. 4 Coupling versus slot spacing for resonant slot
$2L_1=2L_2=\lambda_o/2$, $W_1=W_2=0.1L_1$, H=0.5b, solid line is
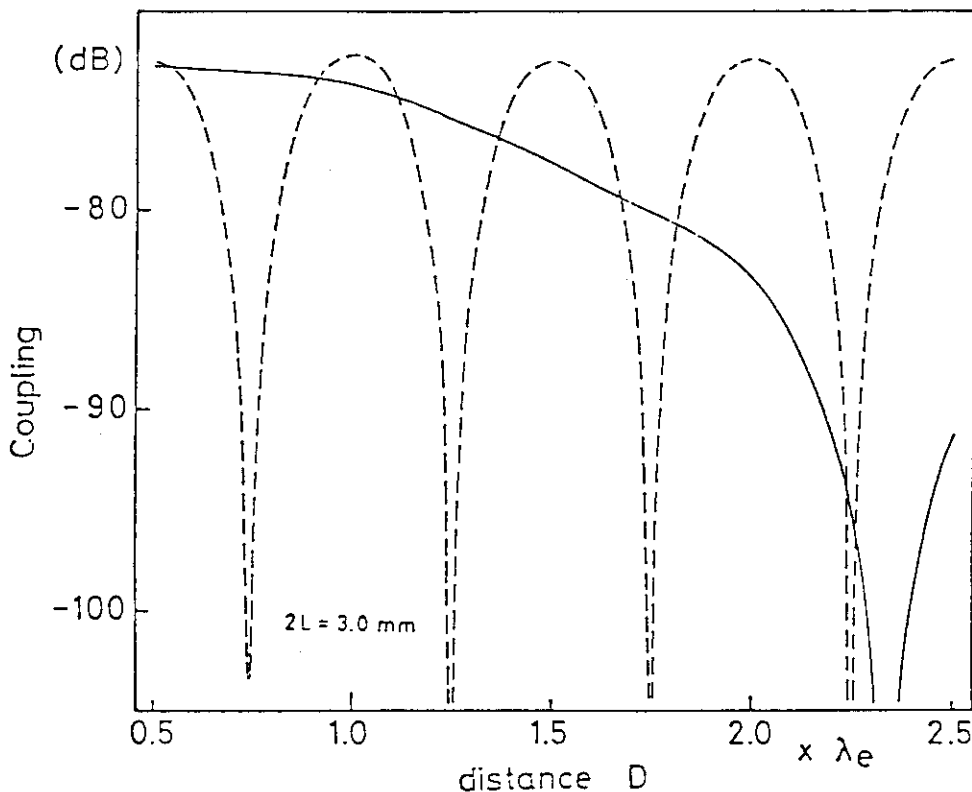forward coupling, dashed line is backward coupling

Fig. 5 Coupling versus slot spacing for non-resonant slot
$2L_1=2L_2=3.0mm$, $W_1=W_2=0.1L_1$, H=0.5b, solid line is
forward coupling, dashed line is backward coupling

Fig. 7 Coupling versus slot width
$2L_1=2L_2=3.0$mm, $W_2=0.1L_1$, $H = 0.5b$, $D = 0.75\lambda_e$, solid line is forward coupling, dashed line is backward coupling
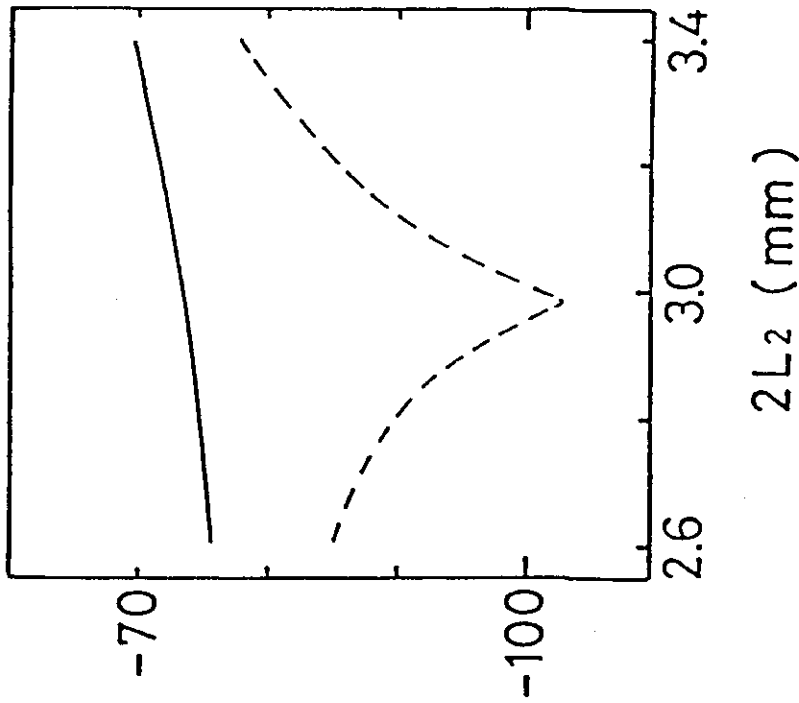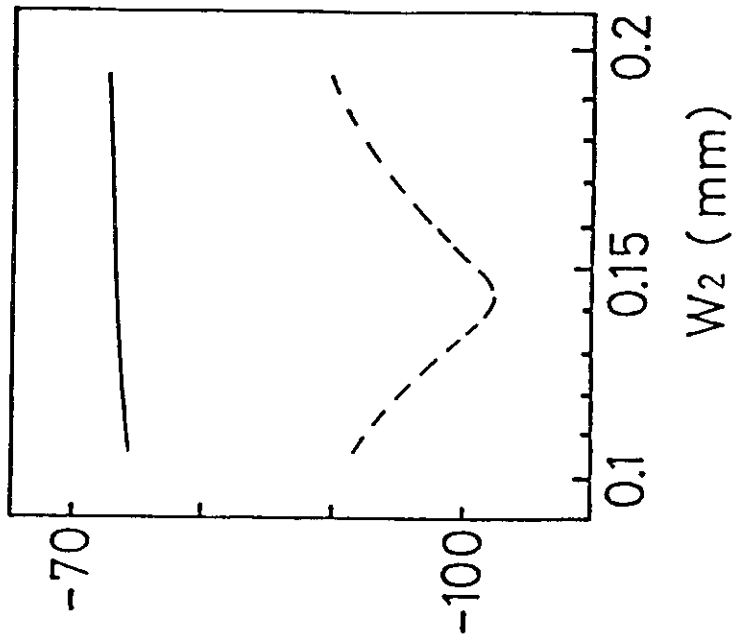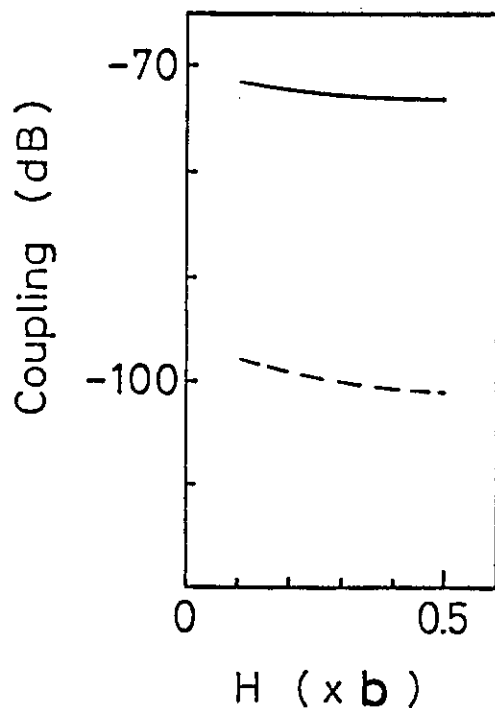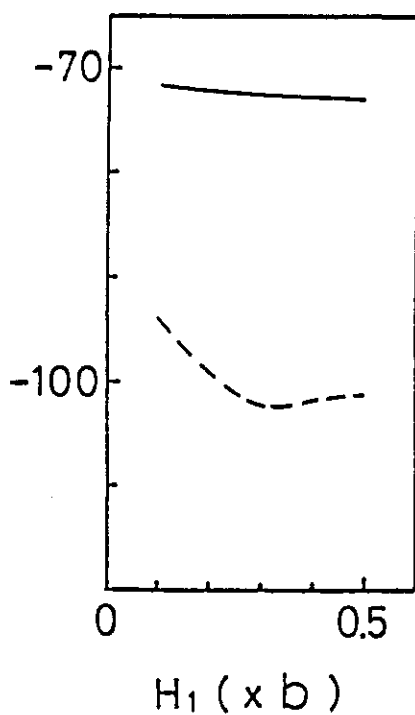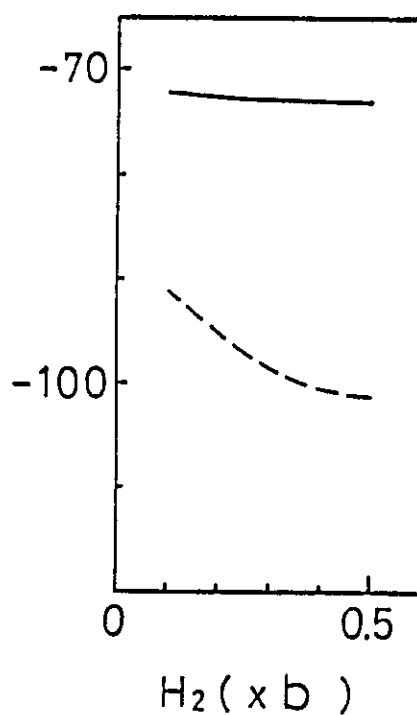

Fig. 6 Coupling versus slot length
$2L_1=3.0$mm, $W_1=0.1L_1$, $W_2=0.1L_2$, $H = 0.5b$, $D=0.75\lambda_e$, solid line is foreard coupling, dashed line is backward coupling

(a) offset of both slots

(b) offset of #1 slot   (c) offset of #2 slot

Fig. 8   Coupling versus slot offset

$2L_1=2L_2=3.0mm$, $W_1=W_2=0.1L_1$, $D=0.75\lambda_e$, solid line is
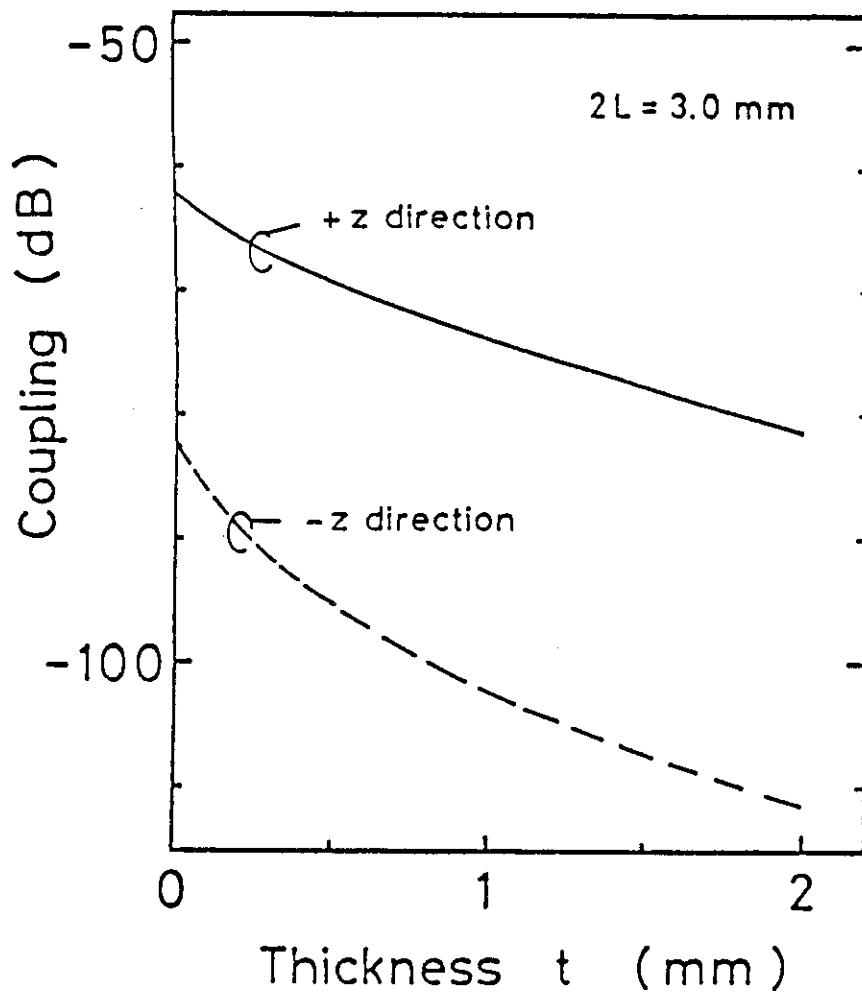
forward coupling, dashed line is backward coupling

Fig. 9 Coupling versus wall thickness t

$2L_1=2L_2=3.0$mm, $W_1=W_2=0.1L_1$, H = 0.5b, D = $0.75\lambda_e$, solid line is forward coupling, dashed line is backward coupling
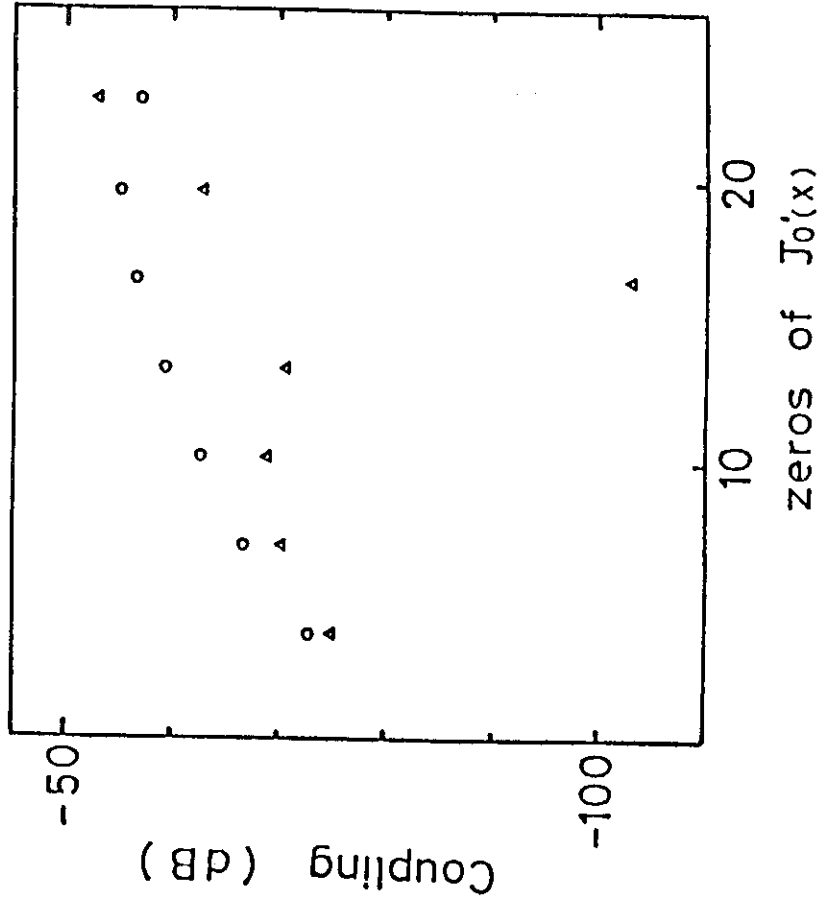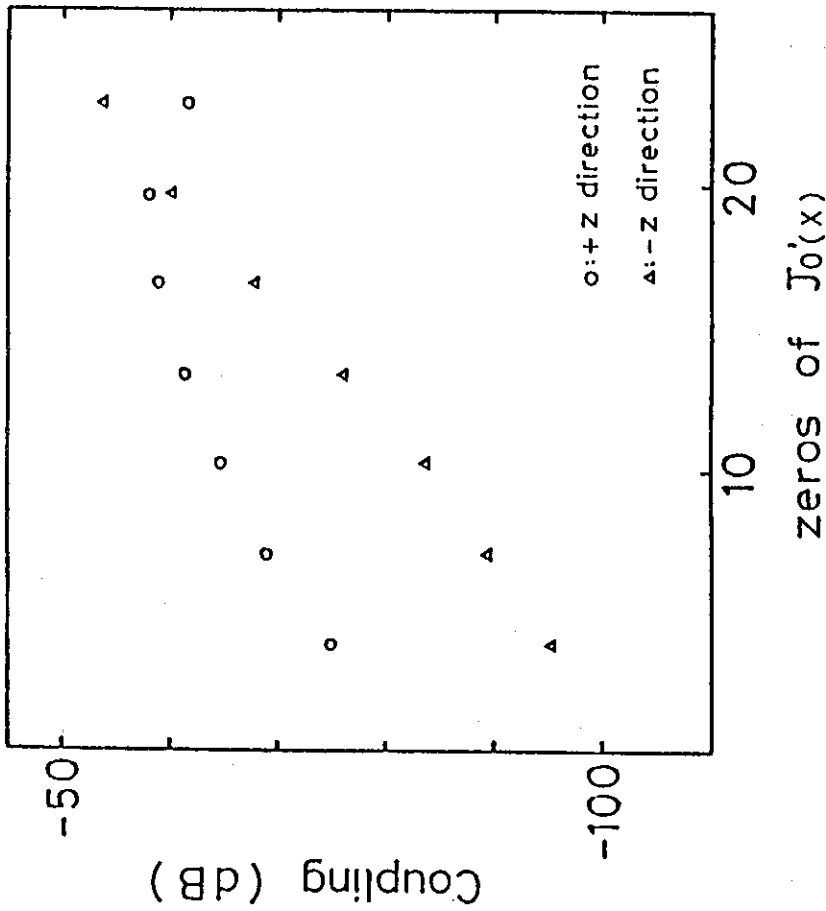
Fig. 12 Coupling versus TE_{0m} mode incident
$2L_1=2L_2=3.0$mm, $W_1=W_2=0.1L_1$, $D=0.75\lambda_e$, $H=0.5b$
o : forward coupling, $\triangle$: backward coupling

Fig. 11 Coupling versus TE_{0m} mode incident
$2L_1=2L_2=3.0$mm, $W_1=W_2=0.1L_1$, $D=0.75\lambda_e$, $H=0.5b$
o : forward coupling, $\triangle$: backward coupling

Appendix A
Generalized admittance ratios and moments of incident magnetic fields

In the notation of GAR's (generalized admittance ratio), the left superscript k, the right ones p, q and the subscripts i, j denote the relevant region, basis functions, and slot number, respectively. Corresponding to various combinations of these super/subscripts, following five members are distinguished.

$${}^{C}Y^{pq}_{jj} \quad : \text{self GAR in circular waveguide}$$

$${}^{C}Y^{pq}_{ij} \quad : \text{mutual GAR in circular waveguide}$$

$${}^{R}Y^{pq}_{jj} \quad : \text{self GAR in rectangular waveguide}$$

$${}^{R}Y^{pq}_{ij} \quad : \text{mutual GAR in rectangular waveguide}$$

$${}^{k,x}y^{pq}_{i} \quad : \text{GAR inside slot region}$$

In this appendix, these GAR's and the moments of incident magnetic fields C_{ip} are evaluated for basis functions given by eqs. (7)-(10). We assume the time variation factor as $e^{j\omega t}$.

It should be noted that GAR's satisfy the following equations because of the reciprocities of dyadic Green's functions.

$${}^{k}Y^{pq}_{} = {}^{k}Y^{qp}_{ji} \tag{A-1}$$

$${}^{k,x}y^{pq}_{ij} = {}^{k,x}y^{qp}_{ji} \tag{A-2}$$

A-1 Self GAR in circular waveguide

In evaluating the self GAR, we used Stevenson's approximation [8] to avoid the singularility of Green's functions.

$${}^{C}Y^{11}_{ii} = \frac{1}{\sin^2 k_o\ell_i} \sum_n \sum_m C_{nm} \times F^1_{nm} - \frac{\cos k_o\ell_i}{\sin^2 k_o\ell_i} \sum_n \sum_m C_{nm}F^2_{nm} + P_1 \tag{A-3}$$

$${}^{C}Y^{12}_{ii} = \frac{1}{\sin k_o\ell_i(1-\cos k_o\ell_i)} \sum_n \sum_m C_{nm} \times F^3_{nm} - \frac{\cos k_o\ell_i}{\sin k_o\ell_i(1-\cos k_o\ell_i)} \sum_n \sum_m C_{nm}F^4_{nm} + P_1$$

$$\tag{A-4}$$

$$C_{Y_{ii}}22 = - \frac{\sin k_o \ell_i}{(1-\cos k_o \ell_i)^2} \sum_n \sum_m C_{nm} F_{nm}^4 + P_2 \tag{A-5}$$

$$C_{Y_{ii}}33 = \frac{1}{\sin^2 k_o \ell_i (1-\cos k_o \ell_i)} \sum_n \sum_m C_{nm} F_{nm}^5 + P_3 \tag{A-6}$$

$$C_{Y_{ii}}13 = 0 \tag{A-7}$$

$$C_{Y_{ii}}23 = 0 \tag{A=8}$$

The terms in above equations are given as follows.

$$C_{nm} = \frac{j2\pi}{A^2} \times \frac{\varepsilon_{on} J_o^2(n\psi_i)\cos^2(n\phi_i)}{(1 - \frac{n^2}{x_{nm}'^2})} \tag{A-9}$$

$$F_{nm}^1 = \frac{k_o}{\Gamma_{nm} k_c^2} e^{-\Gamma_{nm}\ell_i} \times (\cosh \Gamma_{nm}\ell_i - \cos k_o \ell_i) \tag{A-10}$$

$$F_{nm}^2 = \frac{1}{\Gamma_{nm}} [\frac{1}{\Gamma_{nm}} e^{-\Gamma_{nm}\ell_i} \sin k_o \ell_i - \frac{k_o^2}{\Gamma_{nm} k_c^2} \sin k_o \ell_i - \frac{k_o}{k_c^2} (\cos k_o \ell_i - e^{-\Gamma_{nm}\ell_i})] \tag{A-11}$$

$$F_{nm}^3 = \frac{k_o}{\Gamma_{nm} k_c^2} [\frac{k_o}{2\Gamma_{nm}} (1 - e^{-2\Gamma_{nm}\ell_i}) - e^{-\Gamma_{nm}\ell_i} \sin k_o \ell_i] \tag{A-12}$$

$$F_{nm}^4 = \frac{1}{\Gamma_{nm}} [\frac{k_o^2}{\Gamma_{nm} k_c^2} \cos k_o \ell_i - \frac{1}{k_c^2} (k_o \sin k_o \ell_i - \Gamma_{nm} e^{-\Gamma_{nm}\ell_i}) - \frac{1}{\Gamma_{nm}} e^{-\Gamma_{nm}\ell_i} \cos k_o \ell_i] \tag{A-13}$$

$$F_{nm}^5 = \frac{k_o}{\Gamma_{nm}k_c^2} e^{-\Gamma_{nm}\ell_i} \times \left[\frac{k_o}{\Gamma_{nm}} (1-\cosh \Gamma_{nm}\ell_i)\sin k_o\ell_i + (1-\cos k_o\ell_i)\sinh \Gamma_{nm}\ell_i \right]$$

$$(A-14)$$

$$P_1 = - \frac{j \, 2\pi \cos k_o\ell_i}{\sin k_o\ell_i} \times \ell n \left(\frac{4\ell_i}{A\psi_i}\right) \tag{A-15}$$

$$P_2 = \frac{j \, 2\pi}{(1-\cos k_o\ell_i)^2} \times (k_o\ell_i - 2\sin k_o\ell_i + \sin k_o\ell_i \cos k_o\ell_i) \, \ell n \left(\frac{4\ell_i}{A\psi_i}\right)$$

$$+ \frac{j\pi}{(1-\cos k_o\ell_i)^2} \{2 k_o\ell_i(\ell n2-1) + 2S_i(k_o\ell_i)\sin^2 k_o\ell_i + S_i(2k_o\ell_i)\cos 2k_o\ell_i$$

$$- [C_i(2k_o\ell_i) - C_i(k_o\ell_i)] \sin2k_o\ell_i\} \tag{A-16}$$

$$P_3 = - \frac{j2\pi}{(1-\cos k_o\ell_i)} \left(\frac{2}{\sin k_o\ell_i} - \frac{k_o\ell_i}{1-\cos k_o\ell_i} \right) \, n \left(\frac{4\ell_i}{A\psi_i}\right)$$

$$- \frac{j\pi}{\sin k_o\ell_i(1-\cos k_o\ell_i)} \{3[C_i(k_o\ell_i)-\ell n(k_o\ell_i)-\gamma]-\ell n2-[C_i(2k_o\ell_i)-C_i(k_o\ell_i)]\cos k_o\ell_i\}$$

$$- \frac{j\pi}{(1-\cos k_o\ell_i)^2} \{2 k_o\ell_i(1+\ell n2) - [C_i(2k_o\ell_i)-C_i(k_o\ell_i)] \sin k_o\ell_i$$

$$- 3S_i(k_o\ell_i)-(1-2\cos k_o\ell_i)[S_i(2k_o\ell_i)-S_i(k_o\ell_i)]\} \tag{A-17}$$

where A is the radius of circular waveguide, and γ, Si(x), Ci(x) are Euler's constant and sin/cosin integral, respectively. The x_{nm} is the m th root of Jn'(x) = 0, and cutoff wavenumber, propagation constant and normalization factor are given as,

$$k_c = \frac{x'_{nm}}{A} \tag{A-18}$$

$$\Gamma_{nm}^2 = k_c^2 - k_o^2 \tag{A-19}$$

$$\varepsilon_{on} = \begin{cases} 1 : n = 0 \\ 2 : n > 0 \end{cases} \tag{A-20}$$

where k_o is the vacuum wavenumber.

A-2 Mutual GAR in circular waveguide

For the sake of reciprocity, we can assume that $z_i < z_j$ without any loss of generality. The final expression is,

$$C_{Y_{ij}}^{pq} = \nu \sum_n \sum_m C'_{nm} T_i^p T_j^q e^{-\Gamma_{nm}(z_j - z_i)} \tag{A-21}$$

where the terms are given as follows.

$$\nu = \begin{cases} 1 & : q = 1,2 \\ -1 & : q = 3 \end{cases} \tag{A-22}$$

$$C'_{nm} = \frac{j2\pi}{A^2} \cdot \frac{\varepsilon_{on} J_o(n\psi_i) J_o(n\psi_j) \cos n\phi_i \cos n\phi_j}{\left(1 - \dfrac{n^2}{x_{nm}'^2}\right)} \cdot \frac{k_o}{\Gamma_{nm} k_c^2} \tag{A-23}$$

$$T_\alpha^1 = \frac{1}{\sin k_o \ell_\alpha} (\cosh \Gamma_{nm} \ell_\alpha - \cos k_o \ell_\alpha) \tag{A-24}$$

$$T_\alpha^2 = \frac{1}{1 - \cos k_o \ell_\alpha} \left(\frac{k_o}{\Gamma_{nm}} \sinh \Gamma_{nm} \ell_\alpha - \sin k_o \ell_\alpha\right) \tag{A-25}$$

$$T_\alpha^3 = \frac{1}{\sin k_o \ell_\alpha} \times \sinh \Gamma_{nm} \ell_\alpha + \frac{1}{1 - \cos k_o \ell_\alpha} \times \frac{k_o}{\Gamma_{nm}} (1 - \cosh \Gamma_{nm} \ell_\alpha) \tag{A-26}$$

$$(\alpha = i,j)$$

A-3 Self GAR in rectangular waveguide

According to the same procedure with that in circular waveguide, self GAR's in rectangular waveguide are defined as follows.

$$R_{Y_{ii}}^{11} = \frac{1}{\sin^2 k_o \ell_i} \sum_n \sum_m R_{nm} F_{nm}^1 - \frac{\cos k_o \ell_i}{\sin^2 k_o \ell_i} \sum_n \sum_m R_{nm} F_{nm}^2 + P_1 \qquad (A-27)$$

$$R_{Y_{ii}}^{12} = \frac{1}{\sin k_o \ell_i (1-\cos k_o \ell_i)} \sum_n \sum_m R_{nm} F_{nm}^3 - \frac{\cos k_o \ell_i}{\sin k_o \ell_i (1-\cos k_o \ell_i)} \sum_n \sum_m R_{nm} F_{nm}^4 + P_1$$

$$(A-28)$$

$$R_{Y_{ii}}^{22} = - \frac{\sin k_o \ell_i}{(1 - \cos k_o \ell_i)} \sum_n \sum_m R_{nm} F_{nm}^4 + P_2 \qquad (A-29)$$

$$R_{Y_{ii}}^{33} = \frac{1}{\sin^2 k_o \ell_i (1 - \cos k_o \ell_i)} \sum_n \sum_m R_{nm} F_{nm}^5 + P_3 \qquad (A-30)$$

Terms in above equations are given as,

$$R_{nm} = \frac{j2\pi^2}{ab} \times \varepsilon_{on} \varepsilon_{om} J_o^2 \left(\frac{n\pi}{b} w_i\right) \cos^2 \frac{n\pi}{b} X_i \qquad (A-31)$$

$$F_{nm}^1 = \frac{k_o}{\Gamma_{nm} k_c^2} e^{-\Gamma_{nm}\ell_i} \times (\cosh \Gamma_{nm}\ell_i - \cos k_o \ell_i) \qquad (A-32)$$

$$F_{nm}^2 = \frac{1}{\Gamma_{nm}}\left[\frac{1}{\Gamma_{nm}} e^{-\Gamma_{nm}\ell_i}\sin k_o \ell_i - \frac{k_o^2}{\Gamma_{nm} k_c^2} \sin k_o \ell_i - \frac{k_o}{k_c^2}(\cos k_o \ell_i - e^{-\Gamma_{nm}\ell_i})\right]$$

$$(A-33)$$

$$F_{nm}^3 = \frac{k_o}{\Gamma_{nm} k_c^2} \left[\frac{k_o}{2\Gamma_{nm}}(1 - e^{-2\Gamma_{nm}\ell_i}) - e^{-\Gamma_{nm}\ell_i} \sin k_o \ell_i\right] \qquad (A-34)$$

$$F_{nm}^4 = \frac{1}{\Gamma_{nm}} [\frac{k_o^2}{\Gamma_{nm}k_c^2} \cos k_o \ell_i - \frac{1}{k_c^2} (k_o \sin k_o \ell_i - \Gamma_{nm}e^{-\Gamma_{nm}\ell_i}) - \frac{1}{\Gamma_{nm}} e^{-\Gamma_{nm}\ell_i} \cos k_o \ell_i]$$

$$(A-35)$$

$$F_{nm}^5 = \frac{k_o}{\Gamma_{nm}k_c^2} e^{-\Gamma_{nm}\ell_i} \times [\frac{k_o}{\Gamma_{nm}} (1-\cosh \Gamma_{nm}\ell_i)\sin k_o \ell_i + (1-\cos k_o \ell_i) \sinh \Gamma_{nm}\ell_i]$$

$$(A-36)$$

$$P_1 = - \frac{j2\pi \cos k_o \ell_i}{\sin k_o \ell_i} \ell n (\frac{4\ell_i}{w_i})$$

$$(A-37)$$

$$P_2 = \frac{j2\pi}{(1-\cos k_o \ell_i)^2} \times (k_o \ell_i - 2\sin k_o \ell_i - \sin k_o \ell_i \cos k_o \ell_i) \, \ell n (\frac{4\ell_i}{w_i})$$

$$+ \frac{j\pi}{(1-\cos k_o \ell_i)^2} \{ 2k_o \ell_i (\ell n2-1)+2S_i (k_o \ell_i)\sin^2 k_o \ell_i +S_i (2k_o \ell_i)\cos 2k_o \ell_i$$

$$- [C_i (2k_o \ell_i)-C_i (k_o \ell_i)] \, \sin 2k_o \ell_i \}$$

$$(A-38)$$

$$P_3 = - \frac{j2\pi}{(1-\cos k_o \ell_i)} (\frac{2}{\sin k_o \ell_i} - \frac{k_o \ell_i}{1-\cos k_o \ell_i}) \, \ell n (\frac{4\ell_i}{w_i})$$

$$- \frac{j\pi}{\sin k_o \ell_i (1-\cos k_o \ell_i)} \{3[C_i (k_o \ell_i)-\ell n(k_o \ell_i)-\gamma]-\ell n2$$

$$-[C_i (2k_o \ell_i)-C_i (k_o \ell_i)]\times \cos k_o \ell_i \}$$

$$- \frac{j\pi}{(1-\cos k_o \ell_i)^2} \{2k_o \ell_i (1+\ell n2)-[C_i (2k_o \ell_i)-C_i (k_o \ell_i)]\sin k_o \ell_i$$

$$-3S_i (k_o \ell_i)-(1-2\cos k_o \ell_i) [S_i (2k_o \ell_i)-S_i (k_o \ell_i)]\}$$

$$(A-39)$$

where a and b are wide/narrow width of the rectangular waveguide, and

A-4　Mutual GAR in rectangular waveguide

In evaluating the mutual GAR's in rectangular waveguide, we assumed the same condition with that of A-2.

$$R_Y{}^{pq}_{ij} = \nu \sum_n \sum_m R'_{nm} \, T^p_i \, T^q_j \, e^{-\Gamma_{nm}(z_j-z_i)} \tag{A-40}$$

where terms in eq. (40) are given as follows.

$$\nu = \begin{cases} 1 & : \quad q = 1, 2 \\ -1 & : \quad q = 3 \end{cases} \tag{A-41}$$

$$R'_{nm} = \frac{j 2\pi^2}{ab} \epsilon_{on} \epsilon_{om} J_o(\frac{n\pi}{b} w_i) J_o(\frac{n\pi}{b} w_j) \cos \frac{n\pi}{b} X_i \, \cos \frac{n\pi}{b} X_j \times \frac{k_o}{\Gamma_{nm} k_c^2} \tag{A-42}$$

$$T^1_\alpha = \frac{1}{\sin k_o \ell_\alpha} \, (\cosh \Gamma_{nm}\ell_\alpha - \cos k_o \ell_\alpha) \tag{A-43}$$

$$T^2_\alpha = \frac{1}{(1-\cos k_o \ell_\alpha)} \, (\frac{k_o}{\Gamma_{nm}} \sinh \Gamma_{nm}\ell_\alpha - \sin k_o \ell_\alpha) \tag{A-44}$$

$$T^3_\alpha = \frac{1}{\sin k_o \ell_\alpha} \times \sinh \Gamma_{nm}\ell_\alpha + \frac{1}{1-\cos k_o \ell_\alpha} \frac{k_o}{\Gamma_{nm}} (1-\cosh \Gamma_{nm}\ell_\alpha) \tag{A-45}$$

$$(\alpha = i, \, j)$$

A-5　GAR inside slot region

$$c_Y{}^{pq}_i = R_Y{}^{pq}_i = - \sum_{n=0,2,4\cdots} \sum_m D_{nm} \cosh \Gamma_{nm} t \, U^p_m(k_o \ell_i) U^q_m(k_o \ell_j) \tag{A-46}$$

$$x_Y{}^{pq}_i = \sum_{n=0,2,4\cdots} \sum_m D_{nm} \, U^p_m(k_o \ell_i) \, U^q_m(k_o \ell_i) \tag{A-47}$$

Terms in above equations are,

$$D_{mm} = j(\frac{\pi}{2})^4 \frac{\varepsilon_{on} \varepsilon_{om}}{w_i \ell_i \sin h \Gamma_{nm} t} \times J_o^2 (\frac{n\pi}{2}) \times \frac{1}{k_c^2} [(\frac{m}{k_o \ell_i})^2 \frac{\Gamma_{nm}}{k_o} - (\frac{n}{k_o w_i})^2 \frac{k_o}{\Gamma_{nm}}]$$

(A-48)

$$U_m^1(x) = \begin{cases} (-1)^{(\frac{m-1}{2})} \times \dfrac{2x^2 \cot x}{(\frac{m\pi}{2})^2 - x^2} & : \quad m = \text{odd} \\ \\ 0 & : \quad m = \text{even} \end{cases}$$

(A-49)

$$U_m^2(x) = \begin{cases} \dfrac{2x^2}{1-\cos x} \cdot \dfrac{1}{(\frac{m\pi}{2})[(\frac{m\pi}{2})^2 - x^2]} \times [(-1)^{(\frac{m-1}{2})} (\frac{m\pi}{2}) \sin x - x] & : \quad m = \text{odd} \\ \\ 0 \qquad : \quad m = \text{even} \end{cases}$$

(A-50)

$$U_m^3(x) = \begin{cases} -\dfrac{4 x^3}{1-\cos x} \times \dfrac{1}{(\frac{m\pi}{2})[(\frac{m\pi}{2})^2 - x^2]} & : \quad m = 2,6,10,14, \ldots\ldots \\ \\ 0 & : \quad m = \text{otherwise} \end{cases}$$

(A-51)

where $k_c^2 = (\frac{n\pi}{2w_i})^2 + (\frac{m\pi}{2\ell_i})^2$, $\Gamma_{nm}^2 = k_c^2 - k_o^2$.

It should be noted that the terms with $(p,q) = (1,3)$ and $(2,3)$ are identically zero.

A-6   Moments of incident magnetic fields

Moments of incident magnetic fields are evaluated for TE_{0m} mode incident in this paper, and are given as follows.

$$C_{ip} = -\frac{j2}{A} (\frac{\pi k_o z_o}{\beta_{om}})^{1/2} \times \frac{1}{k_c} e^{-j\beta_{om} z_i} \times M_p$$

(A-52)

where

$$k_c = (\frac{x'_{om}}{A}) , \quad \beta_{om}^2 = k_o^2 - k_c^2 \tag{A-53}$$

$$M_1 = \frac{1}{\sin k_o \ell_i} (\cos \beta_{om} \ell_i - \cos k_o \ell_i) \tag{A-54}$$

$$M_2 = \frac{1}{1 - \cos k_o \ell_i} (\frac{k_o}{\beta_{om}} \sin \beta_{om} \ell_i - \sin k_o \ell_i) \tag{A-55}$$

$$M_3 = j \times [\frac{1}{1 - \cos k_o \ell_i} \times \frac{k_o}{\beta_{om}} (1 - \cos \beta_{om} \ell_i) - \frac{1}{\sin k_o \ell_i} \times \sin \beta_{om} \ell_i] \tag{A-56}$$

Appendix B Coupling power in rectangular waveguide

We can evaluate the coupling power by the real part of Poynting power in rectangular waveguide, because the incident magnetic fields are normalized [9]. The final expression of forward and backward coupling power are given as follows.

$$
P^{+} = \frac{2k_{o}b}{a\beta z_{o}} \left| \sum_{k=1}^{N} j(v_{k1}P_{k1} + v_{k2}P_{k2} - v_{k3}P_{k3})e^{j\beta z_{k}} \right|^{2} \tag{A-57}
$$

$$
P^{-} = \frac{2k_{o}b}{a\beta z_{o}} \left| \sum_{k=1}^{N} j(-v_{k1}P_{k1} - v_{k2}P_{k2} + v_{k3}P_{k3})e^{-j\beta z_{k}} \right|^{2} \tag{A-58}
$$

where, the superscripts +, − denote the forward/backward coupling power, respectively. In eqs. (A-57), (A-58), v's are the expansion coefficient of slot aperture rectangular waveguide side, and other terms are given as follows.

$$
P_{k1} = \frac{\cos(\beta \ell_{k}) - \cos(k_{o}\ell_{k})}{\sin(k_{o}\ell_{k})} \tag{A-59}
$$

$$
P_{k2} = \frac{(k_{o}/\beta)\sin(\beta \ell_{k}) - \sin(k_{o}\ell_{k})}{1 - \cos(k_{o}\ell_{k})} \tag{A-60}
$$

$$
P_{k3} = \frac{\sin(\beta \ell_{k})}{\sin(k_{o}\ell_{k})} - \frac{k_{o}(1 - \cos(\beta \ell_{k}))}{\beta(1 - \cos(k_{o}\ell_{k}))} \tag{A-61}
$$

$$
\beta = \sqrt{k_{o}^{2} - (\pi/a)^{2}} \tag{A-62}
$$